AGU PUBLICATIONS

JGR

Journal of Geophysical Research: Atmospheres

RESEARCH ARTICLE
10.1002/2017JD027615

Key Points:
- To implement optimized fuzzy logic method to deduce ABL heights from the new LAWP
- To describe the CBL characteristics (diurnal and seasonal) over the Gadanki region
- Diurnal and seasonal variabilities of the CBL of the radar are compared and validated with surface temperature measured by a collocated AWS

Supporting Information:
- Supporting Information S1

Correspondence to:
S. Venkatramana Reddy and S. Allabakash, drsvreddy123@gmail.com; shaik@kict.re.kr

Citation:
Allabakash, S., P. Yasodha, L. Bianco, S. Venkatramana Reddy, P. Srinivasulu, and S. Lim (2017), Improved boundary layer height measurement using a fuzzy logic method: Diurnal and seasonal variabilities of the convective boundary layer over a tropical station, *J. Geophys. Res. Atmos.*, *122*, 9211–9232, doi:10.1002/2017JD027615.

Received 16 AUG 2017
Accepted 17 AUG 2017
Accepted article online 4 SEP 2017
Published online 8 SEP 2017

Improved boundary layer height measurement using a fuzzy logic method: Diurnal and seasonal variabilities of the convective boundary layer over a tropical station

S. Allabakash[1], P. Yasodha[2], L. Bianco[3,4], S. Venkatramana Reddy[5], P. Srinivasulu[6], and S. Lim[1]

[1]Korea Institute of Civil Engineering and Building Technology, Ilsan, South Korea, [2]National Atmospheric Research Laboratory, Department of Space, Gadanki, India, [3]Cooperative Institute for Research in Environmental Sciences (CIRES), Boulder, Colorado, USA, [4]NOAA/Earth System Research Laboratory/Physical Sciences Division, Boulder, Colorado, USA, [5]Department of Physics, Sri Venkateswara University, Tirupati, India, [6]Astra Microwave Products Limited, Hyderabad, India

Abstract This paper presents the efficacy of a "tuned" fuzzy logic method at determining the height of the boundary layer using the measurements from a 1280 MHz lower atmospheric radar wind profiler located in Gadanki (13.5°N, 79°E, 375 mean sea level), India, and discusses the diurnal and seasonal variations of the measured convective boundary layer over this tropical station. The original fuzzy logic (FL) method estimates the height of the atmospheric boundary layer combining the information from the range-corrected signal-to-noise ratio, the Doppler spectral width of the vertical velocity, and the vertical velocity itself, measured by the radar, through a series of thresholds and rules, which did not prove to be optimal for our radar system and geographical location. For this reason the algorithm was tuned to perform better on our data set. Atmospheric boundary layer heights obtained by this tuned FL method, the original FL method, and by a "standard method" (that only uses the information from the range-corrected signal-to-noise ratio) are compared with those obtained from potential temperature profiles measured by collocated Global Positioning System Radio Sonde during years 2011 and 2013. The comparison shows that the tuned FL method is more accurate than the other methods. Maximum convective boundary layer heights are observed between ~14:00 and ~15:00 local time (LT = UTC + 5:30) for clear-sky days. These daily maxima are found to be lower during winter and postmonsoon seasons and higher during premonsoon and monsoon seasons, due to net surface radiation and convective processes over this region being more intense during premonsoon and monsoon seasons and less intense in winter and postmonsoon seasons.

1. Introduction

The atmospheric boundary layer (ABL) is the lowest part of the atmosphere that lies between the Earth's surface and free atmosphere. Surface forcings such as thermal heat, momentum, and moisture fluxes are strong within the ABL [*Stull*, 1988], and hence, the height of ABL depends on these parameters. Turbulence and other transport processes, as well as diffusion of air pollutants, take place in this layer, and for this reason, they are highly dependent on the ABL structure. The amount of net surface radiation received at the Earth's surface varies diurnally as well as seasonally, and the corresponding changes in surface temperature affect the ABL structure and its growth. The development of the ABL is also subjective to topographic features, atmospheric conditions, soil type, agricultural practices, etc. [*Stull*, 1988; *Garratt*, 1992; *Medeiros et al*., 2005]. Hence, knowing the behavior of the ABL is important to better understand and predict the changes in weather locally and regionally, for natural hazard identification, climate modeling, now casting, and air quality modeling [*Stull*, 1988; *Garratt*, 1992]. The role of the ABL can be even more prominent over tropical regions, where convection is stronger than in other parts of the world [*Reddy et al*., 2012]. On nominal clear-sky days (which we hereafter define as days with more than 50% of the integrated daytime insolation [*Reno et al*., 2012], which lead to strong convection driven principally by solar heating), the ABL height has a well-defined structure and diurnal cycle, leading to the development of a convective boundary layer (CBL) during the day time and of a stable boundary layer, which can be capped by a residual layer, during the nighttime [*Stull*, 1988].

In situ observation systems like radiosonde, meteorological towers, and remote sensing systems like SOund Detection And Ranging, Radio Acoustic Sounding System (RASS), and LIght Detection And Ranging (LIDAR) have been used to describe the ABL structure [*Contini et al*., 2004; *Emeis et al*., 2004; *Coulter*, 1979;

Basha and Venkat Ratnam, 2009]. These systems can characterize the ABL structure but have low height coverage (meteorological towers, RASS, and LIDAR) or coarser temporal and spatial resolutions (radiosonde). Hence, it is difficult to routinely detail the structure of the ABL [*Stull*, 1988; *Garratt*, 1992]. Wind profiling (WP) radars are also robust remote sensing instruments used to characterize the structure of the boundary layer with excellent height and temporal resolutions [*White et al*., 1991a, 1991b].

The variations in the ABL height over the Gadanki region (located in southeast India) using a Lower Atmospheric Wind Profiler (LAWP) were first investigated by *Reddy et al*. [2002]. *Krishnan et al*. [2003] attempted to study diurnal variations of the ABL over Gadanki for some case studies using the same LAWP. *Reddy et al*. [2006] analyzed the variation of the boundary layer during days classified as descent (CBL decreases in late afternoon hours), ascent (CBL continues to ascend after midday also), or inversion layer days (CBL elevated throughout the day; inversion layer persists between 1.5 and 3.5 km). *Kalapureddy et al*. [2007] analyzed the diurnal and seasonal variability of the turbulence kinetic energy (TKE) dissipation rate in the ABL over Gadanki and reported larger TKE during summer and monsoon seasons and smaller TKE in postmonsoon and winter seasons. Karanam Kishore *Kumar and Jain* [2006] reported CBL variations during dry convection (nonprecipitating) days (CBL gradually increases in morning hours and drastically decreases in evening hours), premonsoon precipitation days (CBL shows a continuously growing trend), and monsoon precipitating days (CBL is shallow and gradually ascending and gradually descending). *Basha and Venkat Ratnam* [2009] presented variations of the ABL height during different seasons based on GPS radio occultation data. In their study they reported maximum ABL heights during premonsoon periods followed by monsoon, postmonsoon, and winter periods. *Reddy et al*. [2012], based on variation of the ozone mixing ratio, observed that the ABL height is smaller on rainy days and deeper on sunny days. In the above mentioned studies using the LAWP measurements over the Gadanki region, as well as in more recent applications, the ABL height has been estimated using the method described by *Angevine et al*. [1994], which hereafter we will refer to as "standard method" and will be explained later in the manuscript. Unfortunately, this method seems in some cases unable to pick the correct ABL height (examples of which will be given later in the manuscript).

In the recent years, a new method was developed based on a fuzzy logic approach to determine the ABL height from WP radar data. Estimation of the boundary layer height using the FL approach was first explored by *Bianco and Wilczak* [2002] using the information from the range-corrected signal-to-noise ratio (RCSNR), which profiles show a peak in correspondence to the boundary layer top. *Bianco et al*. [2008] expanded the FL method to identify the CBL height using RCSNR, as well as information on the Doppler spectral width of the vertical velocity, and vertical velocity itself. Due to the convective motion, in fact, the variance of the vertical velocity is larger inside the boundary layer where many up- and down-drafts are present, decreasing at the top, giving an indication on the boundary layer height. The Doppler spectral width of the vertical velocity is also an indicator of the presence of turbulence [*McCaffrey et al*., 2016], which is more evident inside the convective boundary layer, decreasing at the top, again helping at inferring where the top of the boundary layer is existed. This FL method (here onward referred to as "original FL method," OFL) has been effectively applied over different sites of California's central valley [*Bianco et al*., 2011]. In the present study, we use the OFL method proposed by *Bianco et al*. [2008], but tuning and optimizing the algorithm to work better for the data collected by the new LAWP in Gadanki [*Srinivasulu et al*., 2012], India, during the years 2011 and 2013. During years 2011 and 2013 the data acquisition was continuous, while during year 2012, we had gaps in the data set, not allowing for a comparison by season, and for this reason, we did not include it in our analysis. Hereafter we will refer to the "tuned FL method" as TFL.

In the present study we present the differences between the "standard method" of *Angevine et al*. [1994], presently used to identify ABL height at this site and with this instrument, the OFL method [*Bianco et al*., 2008], and the TFL method. The main objectives of the present study are to show that the optimized fuzzy logic method is better at deducing ABL heights from the new LAWP located in Gadanki and to use these estimations to describe the characteristics (diurnal and seasonal) of the CBL over the Gadanki region.

The manuscript is organized as follows: section 2 presents the data set used in this study, the "standard method," and the FL approaches used to determine ABL heights. The results of the comparison between the ABL heights estimated by these methods and those obtained using Global Positioning System Radio Sonde (GPS RS) potential temperature profiles are presented in section 3. Also in this section, diurnal and

Table 1. Important specifications of the LAWP System

Parameter	Value
Frequency	1280 MHz
Technique	Doppler Beam Swinging (DBS)
Number of beams	5 (east, west, zenith, north, and south)
Peak Power	1.2 kW at max duty ratio of 10%
Antenna	16 × 16 array (2.8 × 2.8 m)
Bandwidth	15 MHz
Pulse width	0.25–8.0 μs
Min height	300 m
Max range coverage	4–7 km
Range resolution	150 m
Time resolution	3 min (for each 1 set of 5 beam directions)
Beam width	5°

seasonal variations of the CBL over the region of interest are presented and discussed. A summary of our findings is presented in section 4.

2. Data Set and Analysis

Gadanki is located in a rural environment, about 120 km northwest of Chennai. The site has complex topography as it is surrounded by hilly terrain, a mix of agriculture and waste lands (lands which are not used/suitable for agriculture), and rural population centers. Its altitude is ~375 m above sea level. All these factors have a large influence on the development of the ABL. All the ABL studies completed over the Gadanki region and described in the previous section were carried out using the data obtained from a LAWP system, a phased array coherent pulsed radar with a peak power aperture product of about 1.2×10^4 W m^2, operating at 1357.5 MHz, established under an Indo-Japanese collaboration. A detailed description of the system is given in *Rao et al*. [2001] and *Reddy et al*. [2001]. This radar is not working presently, and a replacement to this system, a new LAWP, was built at the National Atmospheric Research Laboratory (NARL), also in Gadanki. This new system operates continuously at 1280 MHz with 256 (16 × 16) antenna elements arranged as planar array. It has a peak power aperture product of 1.2×10^4 W m^2 with a maximum duty ratio of 10% and can probe the atmosphere up to about 4–7 km on clear-sky days. A detailed description of the system is presented in *Srinivasulu et al*. [2012], while important specifications are summarized in Table 1. This radar has been operational since August 2010. Collocated GPS RS (RS-92, Meisei RS-01GII) data are used to validate the ABL heights estimated by the LAWP radar for years 2011 and 2013. During these 2 years the radar operated for 697 days (system maintenance happened during the remaining days). For the present study we discarded the days with weak SNR, days with precipitation/dense clouds, and days with large gaps in the data. Based on these criteria, we selected only the clear-sky days for boundary layer height estimations. A detailed summary (month by month) of selected LAWP data used in the present study is provided in Table 2.

GPS RS launches happen operationally every day at ~17:00 local time (LT), unless some problem arises. For the period of 2011 and 2013, a total of 581 launches were available. ABL heights can be estimated from GPS RS data looking for inversions in the potential temperature profiles and also from water vapor mixing ratio or refractivity [*Basha and Venkat Ratnam*, 2009] in tropical latitudes. In the present study the height of the inversion in the potential temperature profile is used to estimate the height of the ABL. We excluded from this study days with no inversion or with weak inversions and days with severe convection or rainy conditions. Among the original 581 days, a total of 223 clear-sky days were selected for ABL height estimations. A detailed summary (month by month) of selected GPR RS data launched at 17:00 LT used in the present study is presented in Table 3. To compare ABL heights derived by the LAWP with those derived by the GPS RS, we looked at simultaneous measurements at 17:00 LT. We found 136 simultaneous measurements of LAWP and GPS RS at 17:00 LT. A detailed summary (month by month) of selected simultaneous measurements is presented in Table 4. During special campaign programs GPS RS were launched 5 times a day (8:00, 11:00, 14:00, 17:00, and 23:00 LT). We found a total of 59 campaign days with five launches a day during 2011 and 2013. A detailed summary (for each launch time) of selected GPS RS data launched during these campaign days and used in the present study is presented in Table 5.

Table 2. Available Days for Each Month of LAWP Data During 2011 and 2013[a]

Month	Jan	Feb	Mar	Apr	May	Jun	Jul	Aug	Sep	Oct	Nov	Dec
Total days	53	55	59	60	62	60	56	60	59	51	60	62
Discarded days	17	25	23	22	27	26	27	37	27	23	28	29
Considered days	36	30	36	38	35	34	29	23	32	28	32	33

[a]Total days available: 697. Discarded days: 311. Considered days: 386.

Table 3. Available Days for Each Month of GPS RS Data Launched at 17:00 LT During 2011 and 2013[a]

Month	Jan	Feb	Mar	Apr	May	Jun	Jul	Aug	Sep	Oct	Nov	Dec
Total days	37	37	58	38	43	58	57	56	53	43	52	49
Discarded days	25	22	29	21	22	39	40	42	35	23	30	31
Considered days	12	15	29	17	21	19	17	14	18	20	22	19

[a]Total days available: 581. Discarded days: 359. Considered days: 223.

Spectral data collected by the LAWP contain clear-air signal (signal backscattered by irregularities in the refractive index of the atmosphere), as well as ground clutter (signal backscattered by stationary targets), other kind of clutter (signal backscattered by moving targets), and radio frequency interference, to name some. Several data processing methods proposed by *Barth et al*. [1994], *Riddle and Angevine* [1992], *Carter et al*. [1995], and *Strauch et al*. [1984] can help at removing these forms of contamination. Advanced data processing techniques using wavelet transform were proposed by *Jordan et al*. [1997], *Lehmann and Teschke* [2001], *Lehtinen and Jordan* [2006], and *Allabakash et al*. [2015b], and fuzzy logic-based methods are used by *Morse et al*. [2002], *Cornman et al*. [1998], *Bianco and Wilczak* [2002], and *Allabakash et al*. [2015a] to mitigate clutter and other forms of contamination. FL methods appear to be very robust at classifying different types of signals based on their characteristics. In this study we first use the FL-based method presented in *Allabakash et al*. [2015a], then we apply a statistical averaging method to eliminate contaminated outlier echoes [*Merritt*, 1995]. After the contamination has been removed, the noise level is computed using the approach described in *Hildebrand and Sekhon* [1974], and finally, an adaptive moments' estimation algorithm [*Anandan et al*., 2005] is implemented on the cleaned spectra to estimate the Doppler spectra moments [*Woodman*, 1985]. A method combining wavelet [*Allabakash et al*., 2015b] and fuzzy logic [*Allabakash et al*., 2015a] techniques is under development and will be adapted to the radar data for future studies, to improve the data quality and to take advantage of both techniques.

Once the moments are correctly estimated we use them to estimate ABL heights. Peaks in the profiles of C_n^2 have been found to correspond to the height of the capping inversion of the ABL [*Wyngaard and LeMone*, 1980; *Fairall*, 1991]. As the RCSNR is directly proportional to C_n^2 [*VanZandt et al*., 1978], RCSNR can be used to define the ABL top. Since the ABL development responds to the surface forcings with a time scale of about 1 h or less, we compute ABL heights over a period of 1 h. Details of the methods ("standard method" and FL) used for measuring the ABL height are given in the following sections.

2.1. "Standard Method"

In this method the first approach is to find the maximum value in the profile of the RCSNR for each vertical scan, and then the median of these values over a certain period of time (half an hour to 1 hour) is computed. The height corresponding to this median value represents the height of the ABL. Alternately, the second approach is to obtain a median profile of the RCSNR over a certain period of time (half an hour to 1 h), and then the maximum in this median profile is selected, designating the height of the ABL. Both the above mentioned approaches provide similar results [*Angevine et al*., 1994], but this method has some limitations: if the previous day's residual layer has strong refractivity values, then this method might select the residual layer as the boundary layer height; or if the entrainment zone is shallow or large, which can lead to uniform RCSNR over a large portion of the atmosphere, then it is difficult for this method to determine the top of the ABL [*Bianco and Wilczak*, 2002]. *Levi et al*. [2011] used the method presented in *Angevine et al*. [1994] to both night- and day-times for a 1290 MHz wind profiler radar located at a site 3.5 km from the coast of Israeli, characterized by strong sea-breeze onset.

2.2. FL Methods

FL approach is a robust method used to classify and differentiate different signals based on their characteristics [*Cornman et al*., 1998; *Klir et al*., 1997; *Morse et al*., 2002; *Bianco and Wilczak*, 2002; *Bianco et al*., 2008;

Table 4. Available Days for Simultaneous Measurements (GPS RS and LAWP) for Each Month at 17:00 LT During 2011 and 2013[a]

Month	Jan	Feb	Mar	Apr	May	Jun	Jul	Aug	Sep	Oct	Nov	Dec
Simultaneous measurements (LAWP and GPS RS)	11	11	11	12	13	12	10	11	11	11	11	12

[a]Total days of simultaneous measurements: 136.

Table 5. Available GPS RS Data, During Special Field Campaigns, for Each Launch Time During 2011 and 2013[a]

Launch Time	8:00 LT	11:00 LT	14:00 LT	17:00 LT	23:00 LT
Number of days	53	53	54	59	55
Discarded days	41	34	35	33	37
Considered days (simultaneous measurements of LAWP and GPS RS)	12	19	19	26	18

[a]Total number of days: 59.

Allabakash et al., 2015a]. Fuzzy logic is different from Boolean logic as it does allow various degree of "truth" other the "0" for false and "1" for true, allowed in Boolean logic. Fuzzy logic involves "membership functions," "logical operators," and "if-then rules" to obtain an output that represents the degree of "truth" for a given input. There are four steps in the fuzzy logic process: (i) fuzzification, (ii) application of fuzzy logical operator, (iii) aggregation, and (iv) defuzzification.

Fuzzification is the first step in the process. The variables selected for input are normalized and transformed into "fuzzified" values through the use of "membership functions." Membership function is a smoothed curve that produces a smoothed output of possible values between 0 and 1 (not necessary exactly equal to 0 for "false" or 1 for "true," as in the Boolean logic). The "fuzzified" value will be closer to a "0" value if the degree of membership is closer to being "false," while it will be closer to a "1" value if the degree of membership is closer to being "true." Fuzzy logical operators ("AND" or "OR") combine the various "fuzzified" values, produced from the different variables selected for input, producing a single value of membership to "truth." The aggregation step takes all truth values and combines them through a set of rules, decided by the user, generating a resultant membership value. Finally, the aggregated value acts as the input for the defuzzification process. This process produces a final output using centroid, bisector, middle of maximum, largest value of maximum, and smallest of maximum methods. In this paper we use the centroid method that picks up the center of the area under the curve. The fuzzy logic steps of the process are given in Figure S1 in the supporting information. The reader can refer to *Sivanandam et al*. [2007] or *Allabakash et al*. [2015a] or to the MATLAB fuzzy logic toolbox [*Matlab fuzzy logic toolbox*, 2013] for a detailed description of these steps.

In the present study, we follow the FL approach of *Bianco et al*. [2008], using the FL process to evaluate the "SNR score," the "spectral width score," and the "vertical velocity score." The procedure used for determining the SNR and spectral width scores is the following: hourly profiles of median and variance of RCSNR are computed, then these profiles are smoothed using a ninth-order Savitzky-Golay (polynomial) smoothing filter [*Savitzky and Golay*, 1964], also referred to as a "digital smoothing polynomial filter." This process results in smoothing the profiles, preserving the location in height and the shape of the peak. Hourly profiles of variance, gradient, and curvature of RCSNR are also evaluated. These hourly profiles of median, variance, gradient, and curvature of RCSNR are then normalized and given as inputs to the fuzzy logic process, which provides in output a vertical profile of "SNR score" using the four steps of the fuzzy logic process mentioned above. A similar procedure is followed for the "spectral width score" determination, where the inputs to the fuzzy logic process are now hourly vertical profiles of RCSNR and Doppler spectral width of the vertical velocity. A "vertical velocity score" is also determined in addition to the "SNR score" and "spectral width score" to evaluate the ABL height. For the vertical velocity score, the radar-derived vertical velocities are first passed through a consensus procedure, which at each height tries to identify a consensus window of 3 m s^{-1} in width, in which at least 50% of the total number of vertical velocity values can be found in a 1 h time interval and uses only these velocities to calculate the hourly variance and median of the vertical velocity. Where the variance of the vertical velocity is large, we expect a smaller probability that the ABL height is at that height, while where values of the variance of the vertical velocity are small, the probability that the ABL height is at that height is greater. The variance of the vertical velocity and vertical wind speeds itself are provided as inputs to the fuzzy logic process to calculate a "vertical velocity score."

2.2.1. Tuning of the FL Method: Why Is It Tuned and What Is Tuned?

Although we use the same FL approach of *Bianco et al*. [2008] (OFL), we have to acknowledge that ABL characteristics can be very different in tropical conditions compared to other geographical location. Moreover, signal spectrum characteristics can be influenced by various factors, and they can vary from location to location depending on the local weather conditions, topography at the radar site, and radar operating parameters [*Morse et al*., 2002]. The site considered in this study has complex topography

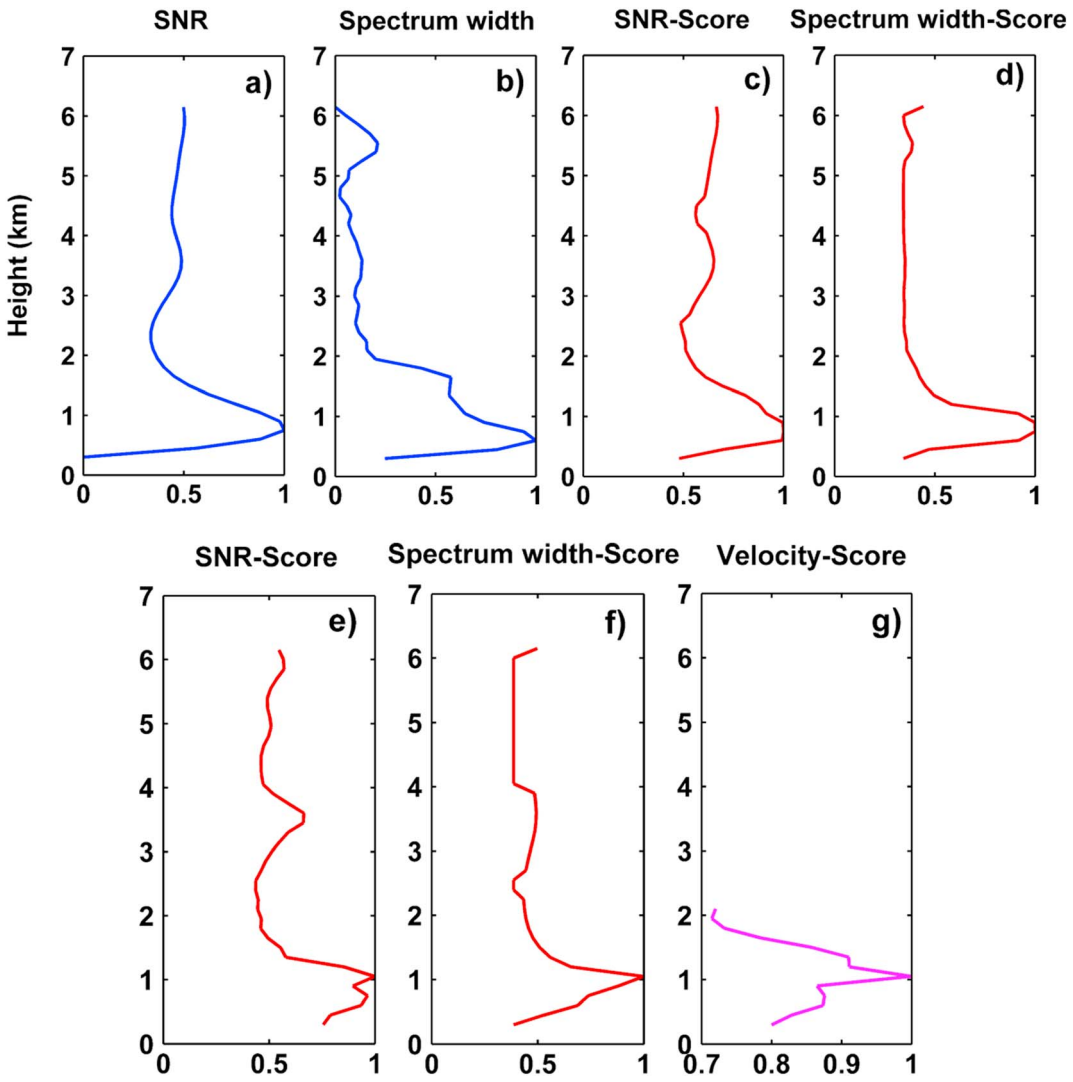

Figure 1. Normalized inputs: (a) range corrected SNR and (b) spectrum width. Outputs of OFL method: (c) SNR score and (d) spectrum width score. Outputs of TFL method: (e) SNR score, (f) spectrum width score, and (g) vertical velocity score.

(with close by mountains); the frequency of the radar and the processing parameters are also significantly different from those of the radars used for the OFL method. Membership functions and rules play an important role at generating the accurate output [*Morse et al.*, 2002]. In our study we found necessary to adjust/tune the membership functions and their parameters, and the if-then rules of the OFL method, to achieve better results.

Initially, a membership function and its parameters are selected based on intuition and knowledge of the typical spectra characteristics. The output ABL height is then compared to independent measurements. If the result is not satisfactory, then the membership functions, their parameters, and the if-then rules are adjusted. This process is iteratively repeated until the comparison is more accurate. In the present study we had to change all the parameters of the membership functions and some of the membership functions as well. Gaussian-shaped, generalized bell-shaped and trapezoidal-shaped membership functions are used for the "SNR score"; Z-shaped, S-shaped, and Gaussian-shaped membership functions are used for the "spectral width score"; Gaussian-shaped membership functions are used for the "vertical velocity score." The if-then rules were also modified to produce a satisfactory output. A detailed description of membership functions and their parameters, and the if-then rules used to determine the "SNR score," "spectral width score," and "vertical velocity score" in the TFL method used in this study are given in the Appendix.

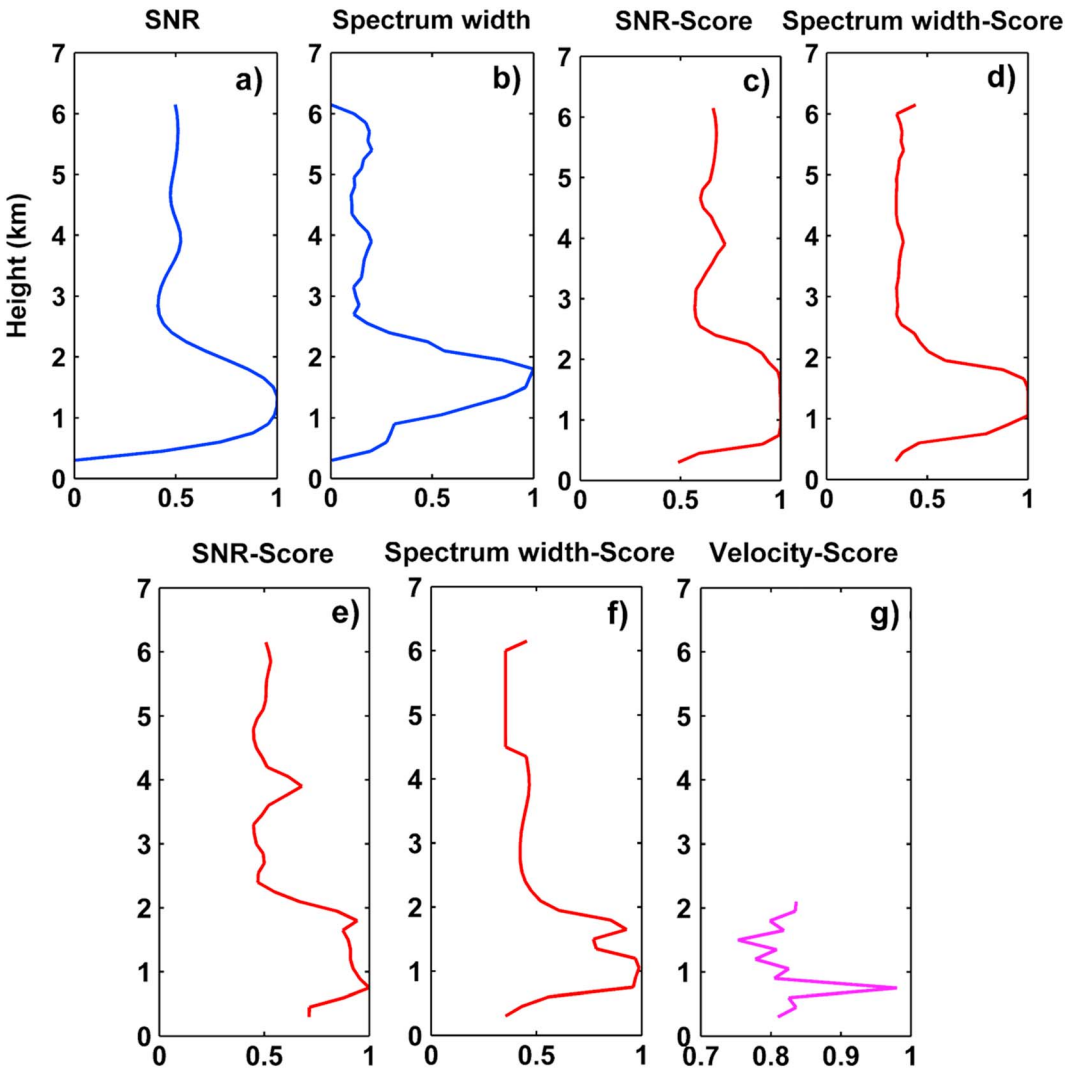

Figure 2. Same as in Figure 1 but for the residual layer case.

2.2.2. Original FL Versus Tuned FL

An example to describe the difference between the OFL and the TFL methods is given for 25 February 2011 at 12:00 LT. The smoothed and normalized inputs (RCSNR and spectrum width) used for the FL process (both OFL and TFL) are shown in Figures 1a and 1b, respectively. The normalized input functions of RCSNR (variance, curvature, and gradient) employed for the OFL method are presented in Figure S2, and the normalized modified input functions of RCSNR (including the vertical velocity profiles) for the TFL method are given in Figure S3. The obtained outputs "SNR score" and "spectrum width score" of the OFL method are shown in Figures 1c and 1d, respectively. The input profiles are in blue, and the profiles of the scores are in red. It can be observed that the RCSNR (Figure 1a) has a maximum around 0.75 km, similarly to all other input parameters (see Figure S2) that also exhibit a significant feature (either maximum or minimum) at that height. As a consequence the "SNR score" and "spectrum width score" both have a maximum value at 0.75 km. Finally, if-then rules are applied to estimate the ABL height at around 0.75 km. Similarly, the outputs (SNR score, spectrum width score, and vertical velocity score) of the TFL method are shown in Figures 1e, 1f, and 1g, respectively. In this case the "SNR score" and "spectrum width score" (in red) present a maximum value at around 1.1 km. Although the "SNR score" exhibits two maxima (at around 0.75 and 1.1 km), the vertical velocity score (obtained from the vertical velocity variance and wind speed) shows only one maximum at around 1.1 km, therefore skewing the ABL height estimation toward that height. From this example (Figure 1), it is clear how a different set of membership functions and if-then rules can generate different outputs.

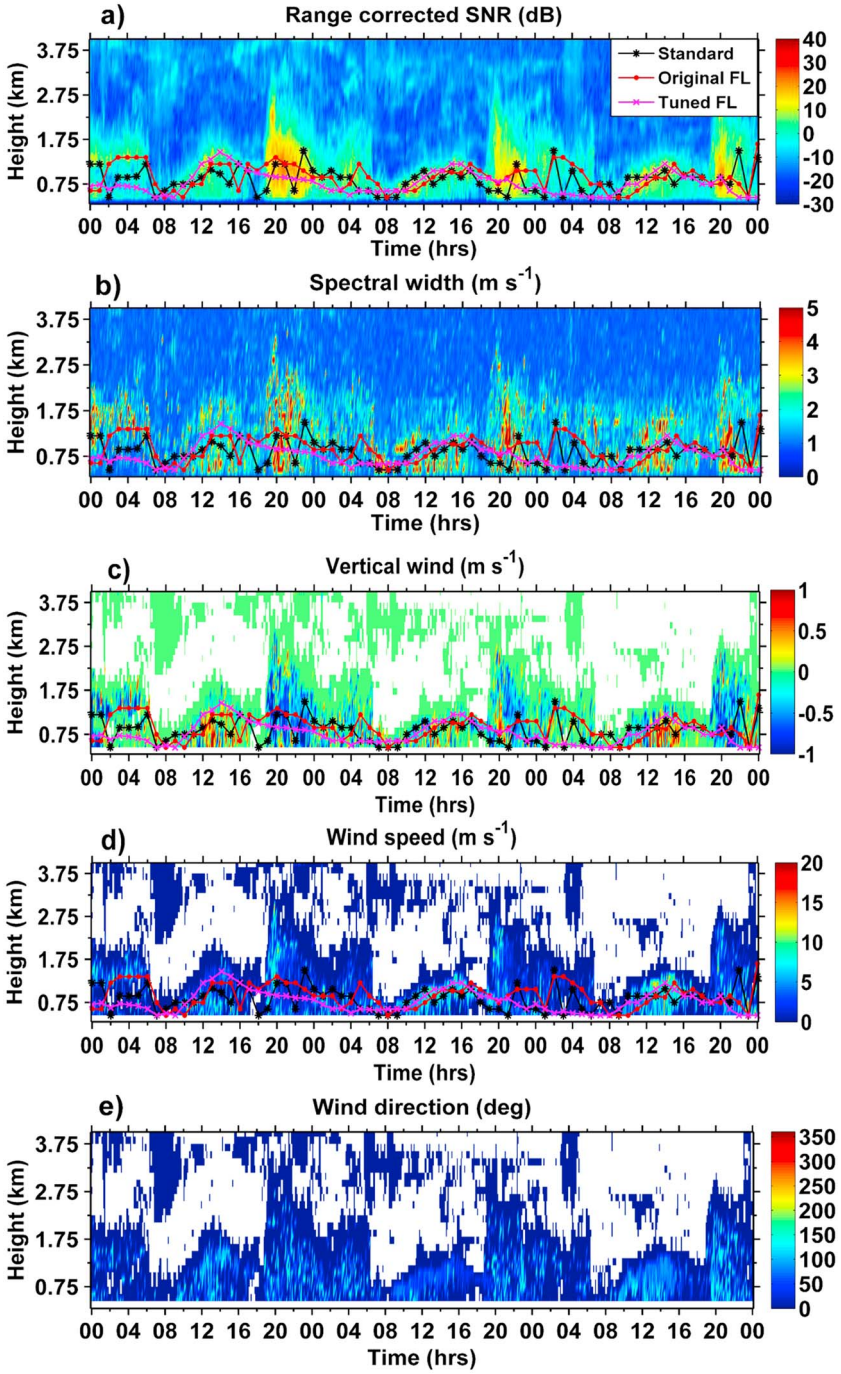

Figure 3. (a) Time-height cross section of RCSNR and ABL height estimation obtained by the standard method (black asterisk markers and solid line), original FL method (red dot markers and solid line), tuned FL method (magenta cross markers and solid line), (b) spectral width of the vertical velocity, (c) vertical velocity, (d) scalar wind speed, and (e) wind direction. All panels are relative to 25–27 February 2011. Time is LT, and ABL height is above ground level.

Another example of the different ABL height estimations between the OFL and TFL methods is given for a residual layer case. This case is relative to 25 February 2011 at 05:30 LT. Figure 2 represents the inputs mentioned before (RCSNR and spectrum width) used for the OFL and TFL processes. The other normalized inputs of the OFL and TFL methods, used for this residual case, are again shown in Figures S4 and S5, respectively. The RCSNR profile (Figure 2a) shows a maximum between 0.75 km and 1.65 km; accordingly, "SNR score" and "spectrum width score" (red profiles) also have maximum values in that range of heights, in both the OFL

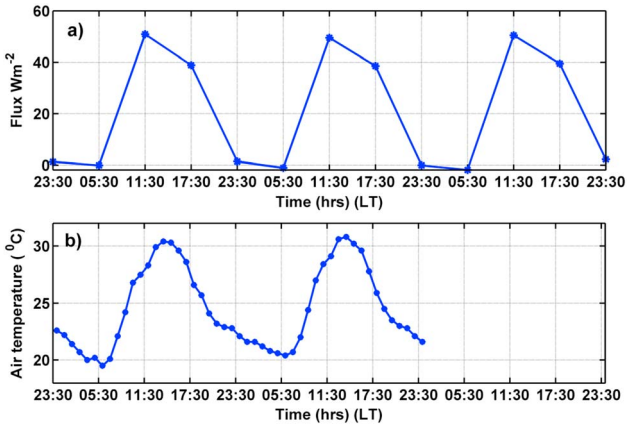

Figure 4. Diurnal variation of (a) surface sensible heat flux (obtained from NCEP reanalysis data) and (b) surface air temperature, observed on 25, 26, and 27 February 2011.

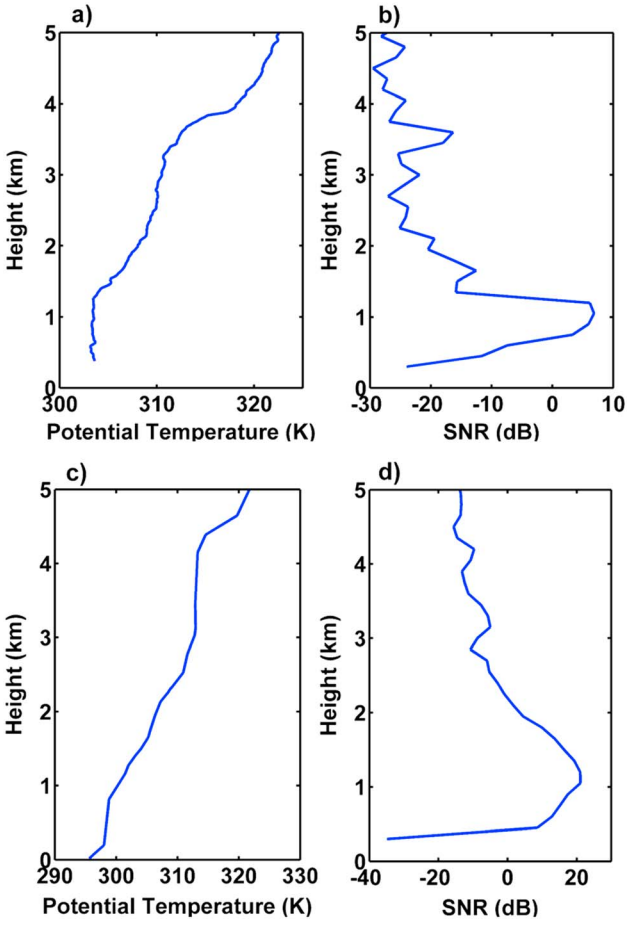

Figure 5. Vertical profiles of (a) potential temperature measured by the GPS RS and (b) RCSNR measured by LAWP on the 26 February 2011 at ~16:45 LT. (c) Potential temperature measured by the atmospheric sounding and (d) RCSNR measured by LAWP, for a residual case on 25 February 2011 at ~05:30 LT.

(Figures 2c and 2d) and TFL (Figures 2e and 2f) methods. In this case it is difficult to compute the ABL height. For this reason in our version of the TFL method, we decided to take into deeper consideration the value of vertical velocity score (Figure 2g shown in magenta), to help in the estimation of the ABL height. While the OFL method estimates the ABL height at 1.2 km, which we will later see is the residual layer, the TFL method places the ABL height at 0.75 km, which we will prove being in better agreement with the independent GPS RS estimations.

The tuning of the membership functions and if-then rules and the better use of the information from the vertical velocity will be proven to improve the ABL height estimations, and these are the efforts we want to highlight in this study.

3. Results and Discussion

In this section we present and quantify the advantages of the TFL method over the "standard method" and the OFL method at identifying the ABL height. Later we will use the CBL estimated by the TFL method to investigate the diurnal and seasonal variations of the CBL daily cycle over Gadanki, India.

3.1. Efficacy of the TFL Method Versus the "Standard Method" and the OFL Method at Estimating ABL Heights

LAWP measurements and relative ABL heights from 25 to 27 February 2011, which include the two example cases presented in the previous section, are presented in Figure 3. Figure 3a shows time-height cross sections of RCSNR and hourly ABL heights as derived by the "standard method" (solid black line and asterisk markers), by the OFL method (solid red line and dot markers), and by the TFL method (solid magenta line and cross markers). Figures 3b–3e represent the Doppler spectral width, vertical wind velocity, scalar wind speed, and wind direction, respectively. We want to mention that we have

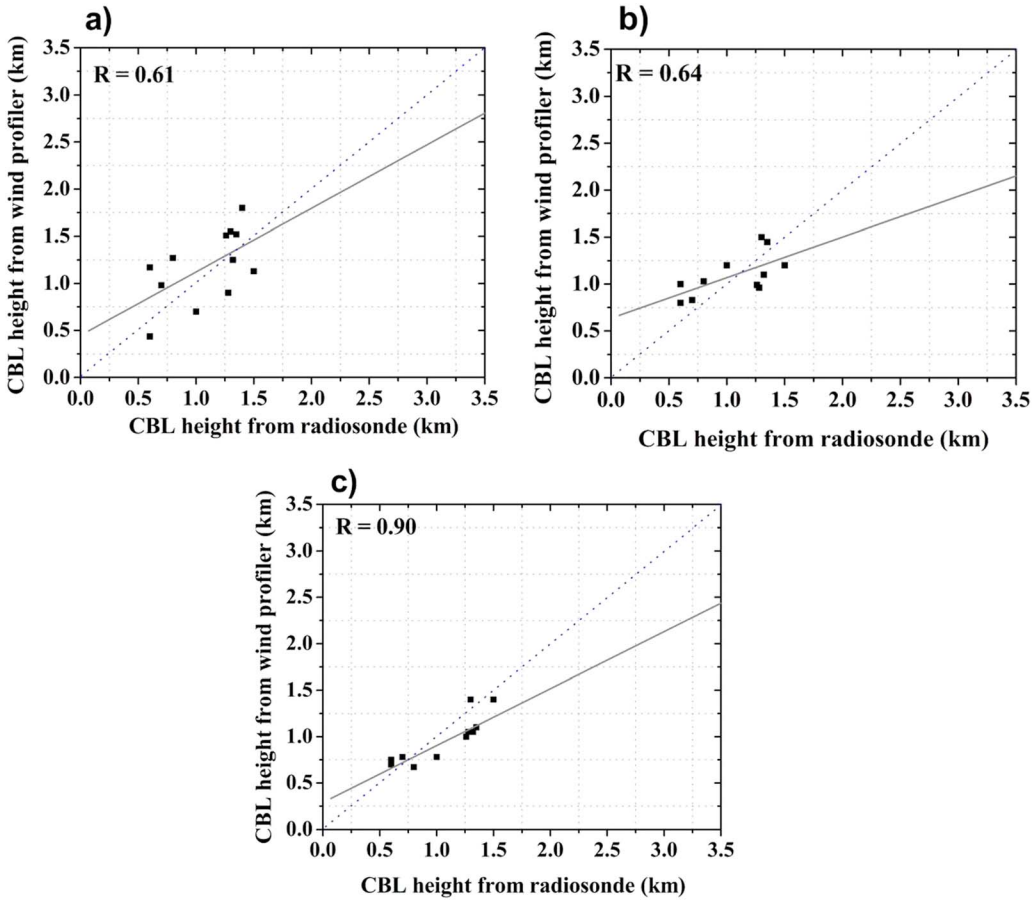

Figure 6. Scatter plots of ABL heights derived from GPS RS measurements (*x* axes) and radar wind profiler estimations (*y* axes) using (a) standard method, (b) original FL method, and (c) tuned FL method at 08:00 LT. ABL height is above ground level.

used a RCSNR threshold value (−15 dB) to plot only vertical wind velocity values (Figure 3c), wind speed (Figure 3d), and wind direction (Figure 3e) relative to larger RCSNR values, to be able to observe interesting features in the ABL. If RCSNR are below the selected threshold, relative values of vertical velocity, wind speed, and wind direction are set as white spaces.

It is worth mentioning that, with our system and at our geographical location, we often noticed large values of RCSNR and spectral width during early night hours, while at the same time, vertical velocity variance values are very low during these periods, associated with large negative vertical velocities (toward the radar). These occurrences are also visible in Figure 3 always around 20:00 LT. Similar evidences were also found by *Sandeep et al*. [2014] that investigated differences and similarities in ABL characteristics between two contrasting episodes of the Indian summer monsoon using measurements from wind profilers and an instrumented 50 m tower at Gadanki in India. This feature is very often present in our radar data, and we suspect that it may be either some atmospheric phenomenon or some strong contamination (for example, from migrating birds). For these occurrences we are expanding our investigation and developing methods to remove it. For this study (although this type of strong SNR and spectral width are still present in our data) we decided to optimize the FL method so that vertical wind speeds are further considered to help distinguish the actual ABL height during this postsunset phenomenon. This further makes our TFL method different from the OFL method. These occurrences are similar in behavior to the residual layer case (which we discussed in the previous section), when we noticed that the information on the wind speed played an important role at estimating the correct ABL height.

It may be observed that the ABL heights estimated using the "standard method" in Figure 3a (in black) present rapid changes in height, which is an atypical feature during clear-sky conditions, as those selected

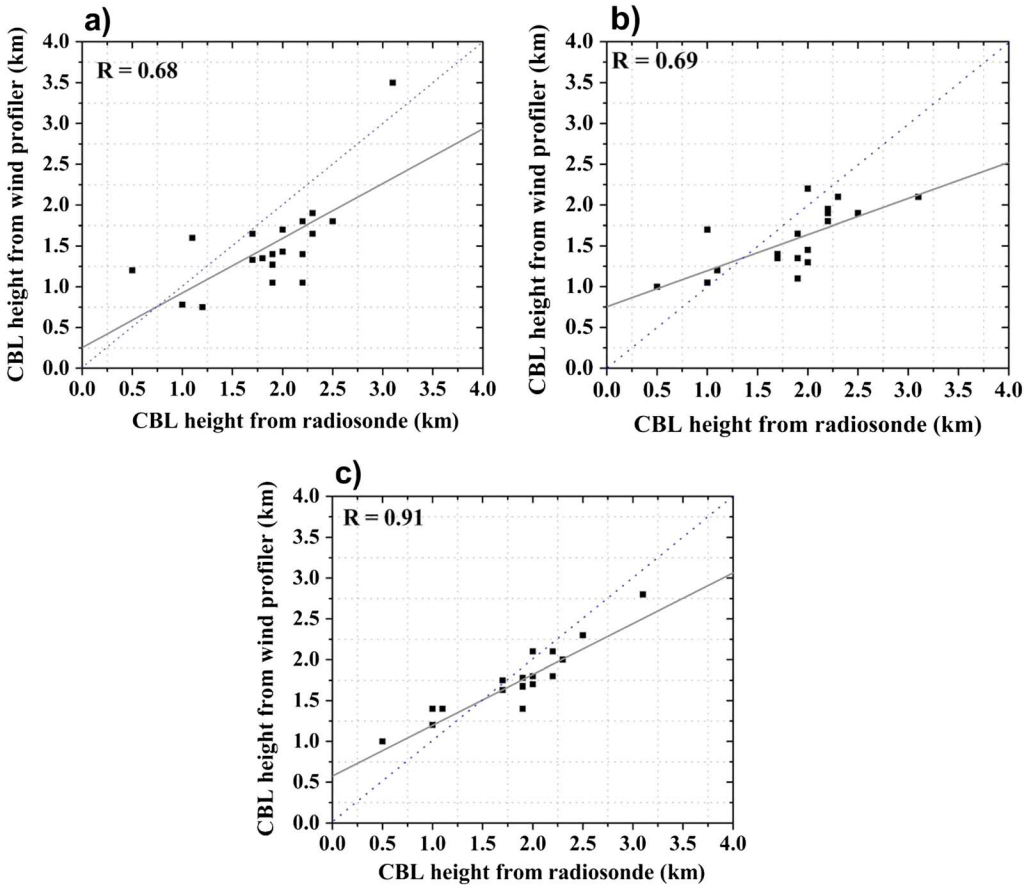

Figure 7. Same as in Figure 6 but for GPS RS launched at 11:00 LT.

for this study. On the other hand, the ABL heights obtained from the OFL method, though varying slowly, seem to produce large values during early night hours. The TFL method estimated ABL heights smoothly varying in time, more realistically during day and nighttimes. The abrupt variations in the ABL height estimated by the "standard method" and high values of ABL estimated by the OFL method are particularly observed around 20:00 LT, when values of RCSNR are strong and vertical velocity values are negative (postsunset phenomenon mentioned before). On some days a peak in the SNR remains visible at high altitude till midnight and even during the night hours, well after the collapse of the CBL. Thermals cease to develop before sunset, allowing turbulence to decay in the formerly well mixed layer, while the layer above still persists as a residual layer [*Stull*, 1988; *Garratt*, 1992]. This is evident in Figure 3 on 25 February 2011, from midnight to early morning hours. The tuning and improvements in the TFL method during such conditions allow more accurate ABL height estimations. The diurnal variations of the ABL height for these 3 days start with a shallower ABL during morning hours, growing steadily up to late afternoon hours and falling down at evening hours. The height of the ABL is relatively constant during nighttimes (from sunset to sunrise). The signatures of the variability of ABL height can also be observed in Figures 3d and 3e of scalar wind speed and direction. This diurnal variability in ABL height compares well to variations in the received net surface radiation, which generate mixing and turbulent transport processes from the Earth's surface to the free atmosphere. In the late evening and night hours the Earth's surface is cooled by radiative cooling and the nocturnal BL gradually replaces the convective mixed layer. From Figure 3 we notice that the ABL reaches a maximum height of ~1.4 km above ground level (agl; between 13:00 and 15:00 LT), 1.3 km agl (between 14:00 to 16:00 LT), and 1.3 km agl (between 13:00 to 14:00 LT) on 25, 26, and 27 February 2011, respectively. In Figure 4a we present the diurnal variation of the surface sensible heat flux on 25, 26, and 27 February 2011, obtained from NCEP reanalysis data for Gadanki region, and Figure 4b indicates the diurnal variation of the surface air temperature on 25 and 26 February 2011,

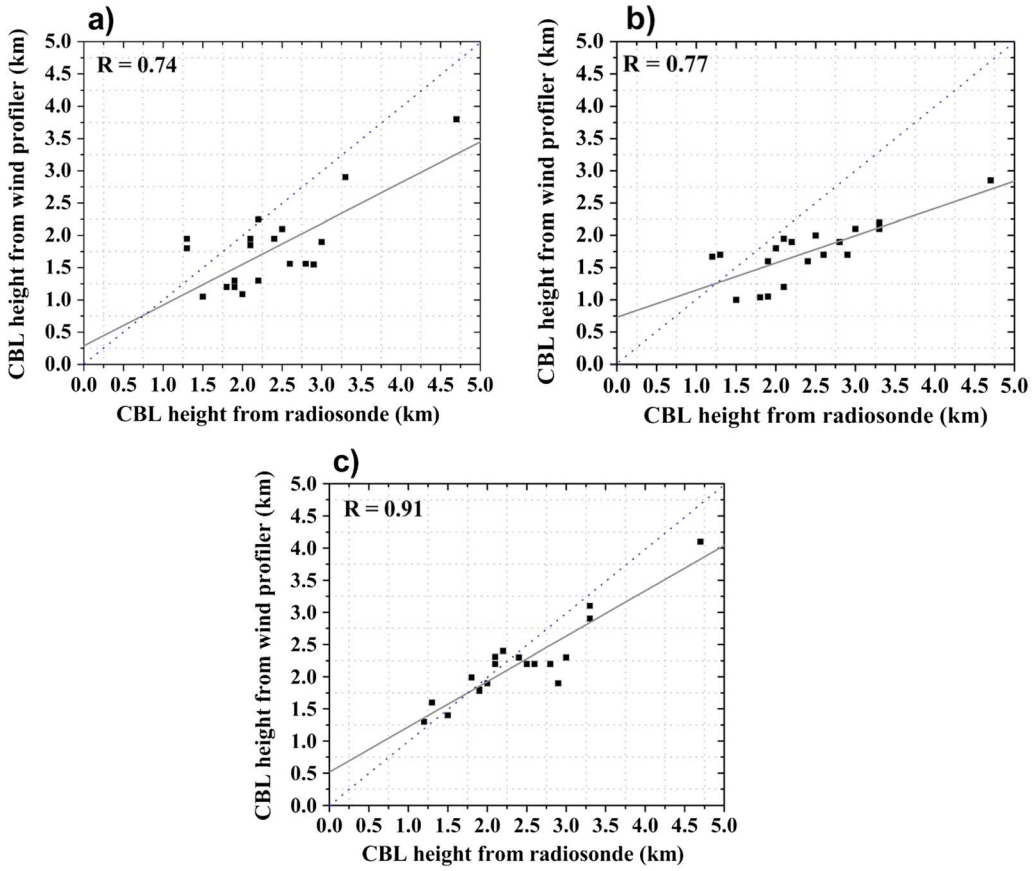

Figure 8. Same as in Figure 6 but for GPS RS launched at 14:00 LT.

obtained from an AWS located at NARL, Gadanki (for 27 February 2011 the AWS data were not available). From Figure 4 we notice maximum fluxes and temperature in agreement with the ABL daily cycles of Figure 3.

We use GPS RS measurements to compute ABL height independently and compare to the "standard," OFL, and TFL methods described before applied to the LAWP measurements. Figure 5 shows an example of a comparison between potential temperature profiles derived from GPS RS measurements (Figure 5a) and RCSNR vertical profiles (Figure 5b) derived from LAWP measurements at ~17:00 LT, on 26 February 2011. The rapid change in the potential temperature profile and the peak in the RCSNR profile at ~1.2 km designates the ABL height. For this example the OFL, TFL, and "standard" methods show similar ABL height estimations (see Figure 3a). Figures 5c and 5d are similar to Figures 5a and 5b but are relative to the residual case at ~05:30 LT on 25 February 2011. For this time, as in situ GPS RS data were not available, we used the data of the atmospheric sounding at the Chennai location (data taken from the university of Wyoming website), as no sounding was available for the Gadanki region. The peak of RCSNR (~1.2 km) differs from the potential temperature inversion (~0.75 km), which indicates that the "standard" and "OFL" methods select the residual layer as ABL height (as mentioned before). For this example the OFL and "standard" methods are unable to select the correct ABL height, while the TFL method selects the actual one. From these examples it is noticeable that there is a good agreement between the GPS RS estimations and those derived from the TFL method applied to the LAWP measurement even in the presence of a residual layer.

We have also looked at other residual layer cases, for example, the one presented in Figure S6, for 7 December 2011 from 20:00 LT to 10:00 LT of the next day. The solid black and red lines connecting the markers show the ABL height identified by the "standard method" and the OFL method, respectively. It

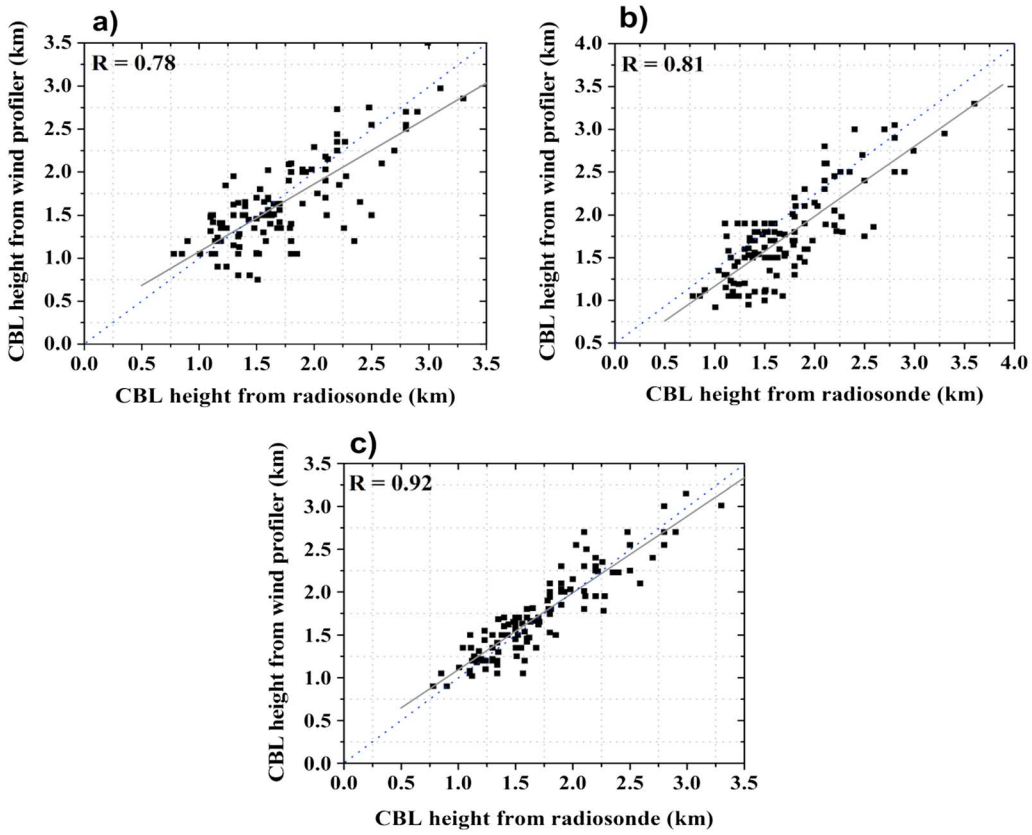

Figure 9. Same as in Figure 6 but for GPS RS launched at 17:00 LT.

can be noticed that these methods select the residual layer as the height of the ABL most of the time. On the other hand, the TFL method can differentiate the residual layer from the ABL and thus identifies the actual ABL height, as shown with the solid magenta line.

Figures 6–10 present one-to-one comparisons between the ABL height estimations from GPS RS potential temperature inversion (*x* axes) and those estimated by the LAWP radar (*y* axes) using the "standard method" (top left), the OFL method (top right), and TFL method (bottom) at 8:00 LT, 11:00 LT, 14:00 LT, 17:00 LT, and 23:00 LT, respectively. The solid lines are the best fit lines. Figures 6–8, and 10 respectively use the GPS RS data collected at 8:00 LT, 11:00 LT, 14:00 LT, and 23:00 LT, launched during the special field campaigns. Figure 9 has more data points as it includes the operational GPS RS launches, happening daily at 17:00 LT. The correlation coefficients are 0.61 (8:00 LT), 0.68 (11:00 LT), 0.74 (14:00 LT), 0.78 (17:00 LT), and 0.48 (23:00 LT) for the "standard method"; 0.64 (08:00 LT), 0.69 (11:00 LT), 0.77 (14:00 LT), 0.81 (17:00 LT), and 0.49 (23:00 LT) for the OFL; and 0.90 (8:00 LT), 0.91 (11:00 LT), 0.91 (14:00 LT), 0.92 (17:00 LT), and 0.88 (23:00 LT) for the TFL method, respectively. From this comparison we can infer that the TFL method estimates the ABL height more accurately than the "standard" and OFL methods over the entire daily cycle.

From Figures 6–10 we can observe that in early morning (08:00 LT) and late evening (23:00 LT) hours, boundary layer heights are below 1.5 km, with few exceptions. We think that these exceptions are due to the presence of strong low level jets (LLJs) detectable at nighttime for those days, over the Gadanki region. Due to the complex terrain surrounding the radar site, the LLJs are strong during night hours generating strong wind shears and associated strong turbulence. This type of deep nocturnal boundary layer (boundary layer from sunset to sunrise referred to as NBL) has also been observed by *Basha and Venkat Ratnam* [2009] and *Manjula et al.* [2016] over this region. *Stull* [1988] also reported that the NBL height is mostly dictated by the radiative cooling at the surface, by the strength of eventually present LLJs and associated turbulence, and residual layer.

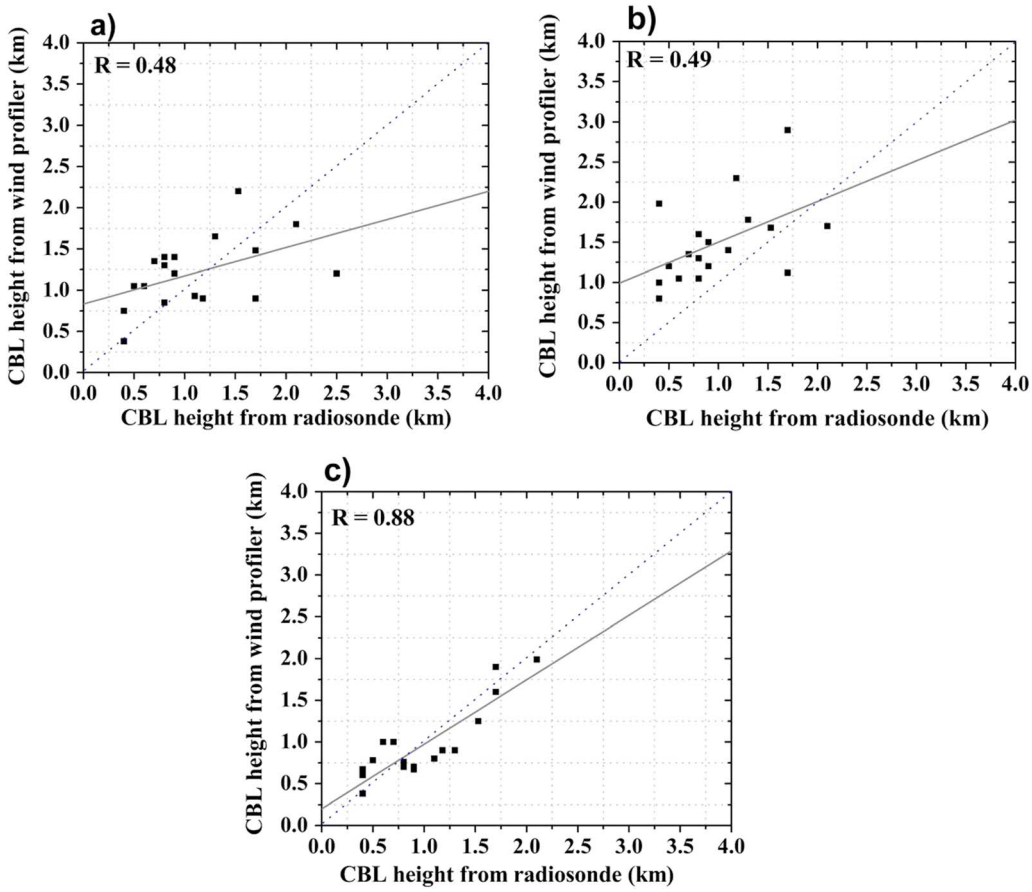

Figure 10. Same as in Figure 6 but for GPS RS launched at 23:00 LT.

3.2. Diurnal and Seasonal Variations of the CBL Daily Cycle Over Gadanki, India

Having established that the TFL method is better at estimating ABL heights at this site and with this instrument, we want to investigate the variability of the daily cycle of the convective boundary layer during the years 2011 and 2013 at the Gadanki site. According to the Indian Meteorological Department (IMD), seasons for the Indian subcontinent region are classified as premonsoon (March, April, and May), monsoon (June, July, August, and September), postmonsoon (October and November), and winter (December, January, and February). Average times for sunrise, local solar noon, and sunset for all the months are shown in Table 6. These times may vary by few minutes (5 to 15 min) from year to year.

Table 6. Sunrise, Local Solar Noon, and Sunset Times for the Various Months

Month	Sunrise (LT)	Solar Noon (LT)	Sunset (LT)
January	~06:30–06:40	~12:10–12:30	~17:50–18:15
February	~06:25–06:38	~12:22–12:29	~18:10–18:20
March	~06:05–06:25	~12:15–12:30	~18:15–18:20
April	~05:45--06:05	~12:00–12:15	~18:20–18:25
May	~05:40–05:50	~12:00–12:10	~18:25–18:40
June	~05:42–06:50	~12:10–12:20	~18:35–18:45
July	~05:49–06:00	~12:15–12:20	~18:40–18:45
August	~06:55–06:05	~12:14–12:20	~18:25–18:40
September	~06:00–06:05	~12:00–12:05	~18:00–18:25
October	~06:02–06:08	~11:55–12:05	~17:45–18:00
November	~06:05–06:20	~11:55–12:00	~17:40–17:45
December	~06:20–06:35	~12:00–12:15	~17:40–17:55

In Figure 11a, we present monthly averaged time-height daily cycles of the CBL from 07:00 LT to 20:00 LT for the year 2011. From this figure, we can observe that the CBL height at 07:00 LT for the different months ranges between 700 m and 1.2 km. We can further notice that, till 09:00 LT, the CBL height is almost constant, while from 09:00 LT to 15:00 LT, the CBL height increases steadily reaching its maximum around 15:00 LT. Later it starts to decay reaching the minimum height at around 19:00–20:00 LT, when the CBL is replaced by the NBL. It can

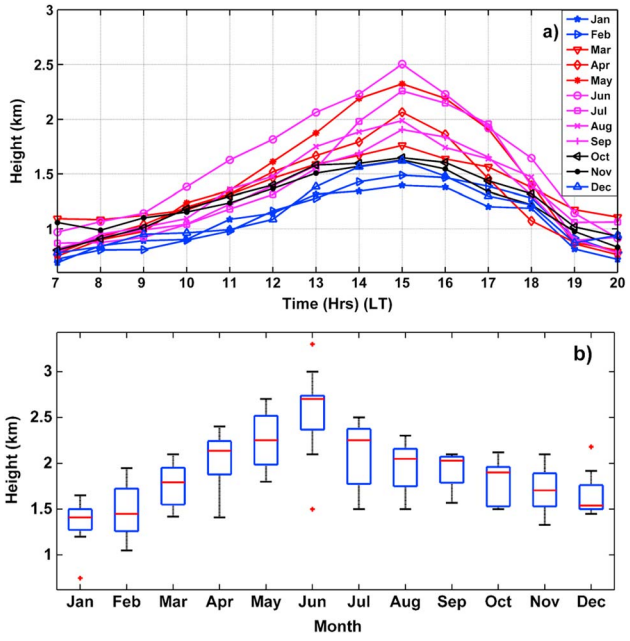

Figure 11. (a) Monthly averaged daily cycles of boundary layer heights for the year of 2011. (b) Box plot of boundary layer height variations measured at 15:00 LT for selected days of each month. The red plus symbols represent outliers that fall outside of the boxes.

also be noted that the maximum height of the CBL varies from month to month, its maximum value being the smallest in January (1.3 km) and the highest in June (2.5 km). We can further notice that CBL height is higher (above 2 km) in premonsoon and monsoon seasons and lower (less than 1.3–1.8 km) in postmonsoon and winter seasons. Figure 11b depicts the height of the CBL at 15:00 LT for all the selected days of each month, for the year 2011. Each box represents the variations of the CBL height and on each box, the red colored mark is the median, and the edges of the box are the 25th (lower edge) and 75th (upper edge) percentiles. This figure also confirms that the CBL height is higher (more than about 1.7 km) in premonsoon and monsoon seasons and lower (less than 1.7 km) in postmonsoon and winter seasons. Data collected during year 2013 are presented in Figure 12. From this figure we notice that the CBL features are similar to those of Figure 11 (year 2011), except that the CBL height reaches its maximum (2.8 km) in the month of May, instead of June. Furthermore, the minimum height of the CBL is 1.5 km, during the month of January, and the maximum height is observed between 14:00 LT and 15:00 LT for all the months. Usually, in south India, solar radiation is larger during the premonsoon season (April and May), increasing the height of the CBL. Hence, the maximum CBL height is observed in May for year 2013. In 2011 the maximum CBL height is observed slightly later, i.e., in June. This may be due to the variation in the onset of the monsoon over Gadanki. The monsoon onset over main land of India (Kerala) usually takes place on 1 June every year and takes about 10 or more days to hit Gadanki. The IMD, Government of India, reported in the year 2013, the progress (advance) of the monsoon was one of the fastest ever, as it took only ~15 days to cover the entire country [*Indian Meteorological Department Monsoon report*, 2013], while in 2011 it took ~45 days [*Indian Meteorological Department Monsoon report*, 2011]. From this, it is inferred that in 2013, monsoon hit Gadanki early than 2011. For this reason, Gadanki region produced higher net surface radiation in June 2011 compared to June 2013. The arrival of monsoon usually generates precipitation. Although we have selected clear-sky days, the precipitation increases soil moisture, which, in turn, changes (reduces) the surface temperature [*Gamo et al*., 1994]. This increase in soil moisture and the decrease of surface temperature as well as the reduced solar irradiance reduce the net surface radiation [*Kohler et al*., 2010], with consequent low surface sensible heat flux and high latent heat flux [*Krishnamurti and Ramanathan*, 1982]. These differences are noted in the different behavior of June 2013, opposite to June 2011. *Krishnamurti and Ramanathan* [1982] also stated that over south India, large net heating takes place (kinetic energy increases) before the monsoon onset (June 2011 in the present study). Therefore, the Bowen ratio (ratio between surface sensible heat flux and latent heat flux) is high in June 2011 and lower in June 2013. Hence, in June 2011 the strong sensible heat fluxes and high Bowen ratios resulted in a deeper CBL than in June 2013 (higher latent heat fluxes and lower Bowen ratio). During postmonsoon and winter seasons the CBL height is shallow for both 2011 and 2013, due to more stable atmosphere and weaker convective activity.

Figures 13a–13d (relative to premonsoon, monsoon, postmonsoon, and winter seasons, respectively) show the hourly averaged seasonal daily cycle of CBL (in blue) and surface temperature (in green). The CBL measured from the radar has been hourly averaged for each season as well as the surface temperature (ST) obtained from the AWS. We observe that the daily cycles of CBL and ST are in good agreement. We also

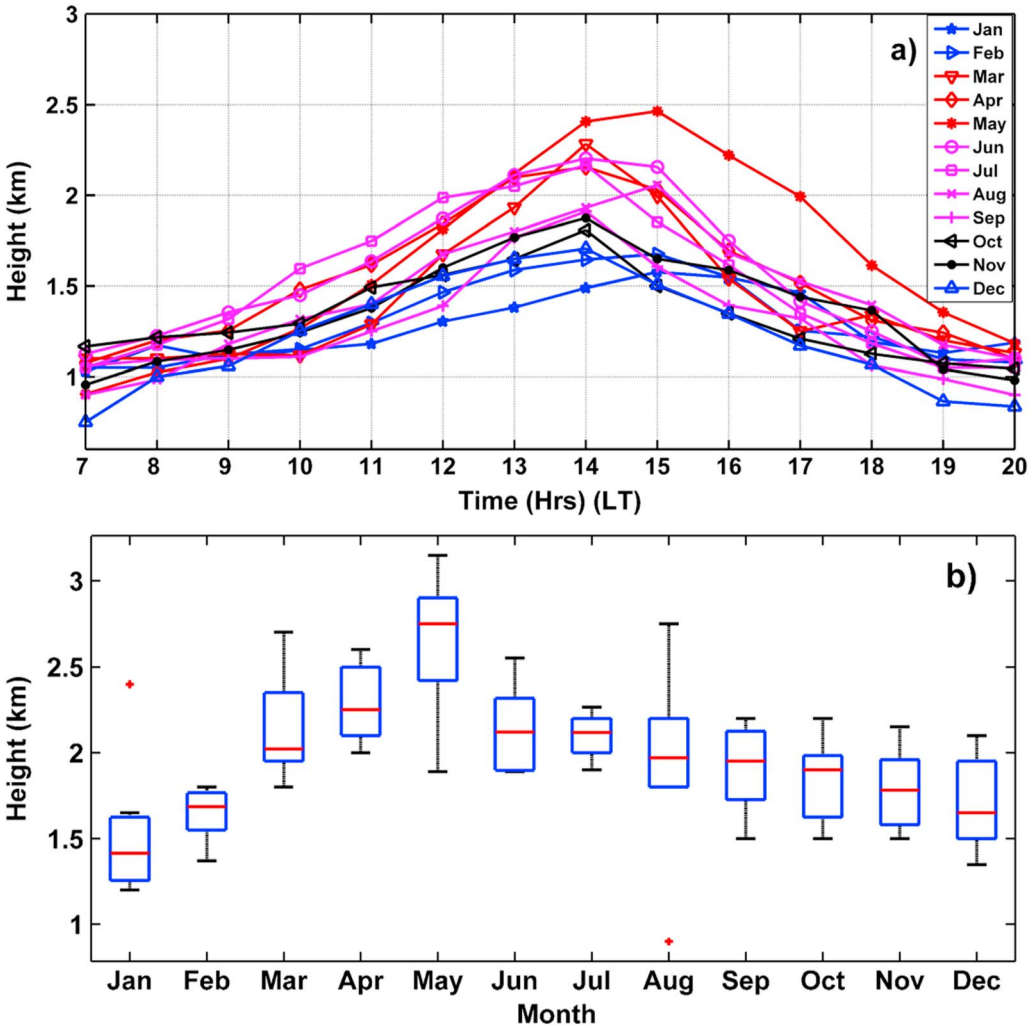

Figure 12. Same as in Figure 11 but for year 2013.

notice that both CBL and ST have maximum values during late afternoon hours and that CBL and ST are maximum in premonsoon season, followed by monsoon, postmonsoon, and winter seasons.

4. Summary

This study shows the advantage of a FL-based method (tuned and optimized to the geographical location and atmospheric radar signal) over the OFL and "standard" methods at identifying the ABL height. The FL methods use the information contained in the range-corrected signal-to-noise ratio, spectral width of the vertical velocity, and vertical velocity itself, improving the estimation of the ABL height. On the opposite, the "standard method" that relies only on the information contained by the RCSNR to identify the ABL height fails at identifying the real ABL height in certain situations, for example, in the presence of a residual layer. Although in our data set we experienced the presence of large SNR and spectral width values late in the day, we optimized the FL method to avoid being deceived by this phenomenon. Nevertheless, we are in the process of investigating the cause for it and we reserve the associated discussion to a future study.

The comparison between the ABL heights estimated by the LAWP radar using standard, OFL, and TFL methods and those obtained from the potential temperature profiles measured by GPS RS launched operationally at the same site at 17:00 LT is also presented, showing correlation coefficients of 0.78, 0.81, and 0.92 for the "standard method," original, and tuned FL methods, respectively. A smaller number of soundings launched during special field campaigns were used to assess the results at different times of the day (8:00, 11:00, 14:00, and 23:00 LT), also demonstrating that the TFL method is more accurate at calculating the ABL

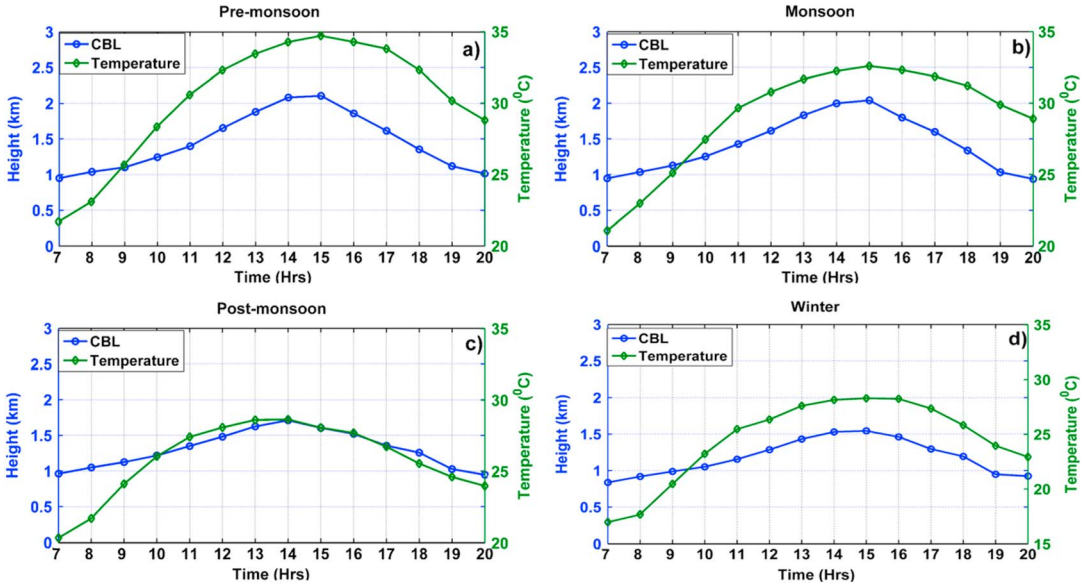

Figure 13. Hourly averaged diurnal variability of CBL and ST during (a) premonsoon, (b) monsoon, (c) postmonsoon, and (d) winter seasons. Time is LT, and ABL height is aboveground level.

heights compared to the standard and OFL methods for this data set. This proves that although the OFL method has advantages in respect to the "standard method," as it uses more information from the radar measurements, its tuning is necessary to optimize its results.

Additionally, the diurnal cycle variations of the CBL computed by the TFL method are studied for years 2011 and 2013, showing that the maximum of the CBL height is always reached at 14:00–15:00 LT. This height decays to a minimum around 19:00–20:00 LT. The diurnal variations are due to the cycle of the net surface radiation and warming of the Earth's surface, which results in rising warm thermals that increase the depth of the CBL. In the late afternoon (17:00–18:00 LT) the decrease in radiative heating lowers the CBL height, which is then replaced by the nocturnal boundary layer. An investigation of the seasonal variation of CBL height shows that the CBL height is higher during premonsoon and monsoon seasons and lower during post-monsoon and winter seasons. The maximum CBL height is observed at ~2.5–3.0 km in premonsoon and monsoon seasons and at ~1.2–1.8 km in winter and postmonsoon seasons. From this analysis it can be inferred that the premonsoon season develops the maximum CBL followed by monsoon, postmonsoon, and winter seasons. We have also compared the hourly averaged CBL and ST for all the seasons showing that the CBL and ST follow the same trend (growing in the noon hours and decaying in the evening hours), and this comparison shows a good agreement in diurnal as well as in seasonal variability.

Appendix A

Four distinct membership function types are used: Gaussian, generalized bell-shaped, trapezoidal, and Z-shaped defined below.

A1. Gaussian Membership Function

$$f(x;\sigma,c) = \exp\left[\frac{-(x-c)^2}{2\sigma^2}\right]$$

A2. Generalized Bell-Shaped Membership Function

The generalized bell function depends on three parameters a, b, and c as given by

$$f(x;a,b,c) = \frac{1}{1+\left|\frac{x-c}{a}\right|^{2b}}$$

where parameter b is usually positive. Parameter c locates the center of the curve. The membership function is evaluated at the points determined by the vector x.

A3. Trapezoidal

The trapezoidal curve is a function of a vector, x, and depends on four scalar parameters a, b, c, and d, as given by

$$f(x;a,b,c,d) = \begin{Bmatrix} 0, & x \le a \\ \left(\frac{x-a}{b-a}\right), & a \le x \le b \\ 1, & b \le x \le c \\ \left(\frac{d-x}{d-c}\right), & c \le x \le d \\ 0, & d \ge x \end{Bmatrix}$$

(OR)

$$f(x;a,b,c,d) = \max\left[\min\left(\frac{x-a}{b-a}, 1, \frac{d-x}{d-c}\right), 0\right]$$

Parameters a and d locate the "feet" of the trapezoid, and parameters b and c locate the "shoulders."

A4. Z-shaped

This spline-based function of x is so named because of its Z-shape. Parameters a and b locate the extremes of the sloped portion of the curve as given by

$$f(x;a,b) = \begin{Bmatrix} 1, & x \le a \\ 1 - 2\left(\frac{x-a}{b-a}\right)^2, & a \le x \le \frac{a+b}{2} \\ 2\left(\frac{x-b}{b-a}\right)^2, & \frac{a+b}{2} \le x \le b \\ 0, & x \ge b \end{Bmatrix}$$

A5. Membership Functions and Parameters for SNR Score Recognition Algorithm

1. SNR score recognition algorithm

For all the mathematical parameters (RCSNR (C_n^2), variance, curvature, and gradient) and SNR score output, Gaussian membership functions are computed and the shape depends on parameters c and σ, which represent the center and width of the curve. Parameter values (c and σ) and rules depend on signal characteristics and site location.

SNR score rules:

1. If RCSNR (C_n^2) is maximum, curvature is maximum, and gradient is middle, then SNR is maximum.
2. If RCSNR (C_n^2) is max2 and curvature is maximum, then SNR is maximum.
3. If RCSNR (C_n^2) is minimum and curvature is minimum, then SNR is minimum.
4. If curvature is minimum and gradient is maximum, then SNR is minimum.
5. If RCSNR (C_n^2) is max2, variance is middle, and curvature is maximum, then SNR is maximum.
6. If RCSNR (C_n^2) is maximum, variance is middle, and gradient is small, then SNR is maximum.
7. If RCSNR (C_n^2) is max2, variance is large, and curvature is minimum, then SNR is minimum.
8. If RCSNR (C_n^2) is max2 and gradient is small, then SNR is maximum.
9. If RCSNR (C_n^2) is maximum, variance is not small, and gradient is not middle, then SNR is maximum.
10. If RCSNR (C_n^2) is max2 and variance is not small, then SNR is maximum.
11. If RCSNR (C_n^2) is maximum, curvature is minimum, and gradient is small, then SNR is maximum.
12. If curvature is minimum and gradient is small, then SNR is maximum.
13. If RCSNR (C_n^2) is minimum, variance is middle, curvature is minimum, and gradient is small, then SNR is maximum.
14. If variance is small, curvature is minimum, and gradient is maximum, then SNR is minimum.
15. If curvature is maximum and gradient is middle, then SNR is maximum.

Table A1. "RCSNR (C_n^2)" Membership Functions and Parameters Used for the SNR Score Recognition

Membership Function	Function Type	Parameter	Parameter	Parameter	Parameter
Min	Gaussian	$\sigma = 363$	$c = 1.3$		
Max	Bell-shaped	$a = 366$	$b = 1.7$	$c = 1023$	
Max2	Trapezoidal-shaped	$a = 1000$	$b = 1013$	$c = 1020$	$d = 1025$

Table A2. "Variance" Membership Functions and Parameters Used for the SNR Score Recognition

Membership Function	Function Type	Parameter	Parameter	Parameter
Small	Gaussian	$\sigma = 370$	$c = 1$	
Middle	Bell-shaped	$a = 635$	$b = 2.1$	$c = 1005$
Large	Bell-shaped	$a = 640$	$c = 2.7$	$c = 1012$

Table A3. "Curvature" Membership Functions and Parameters Used for the SNR Score Recognition

Membership Function	Function Type	Parameter	Parameter
Min	Gaussian	$\sigma = 351$	$c = 0.8$
Max	Gaussian	$\sigma = 1012$	$c = 246$

Table A4. "Gradient" Membership Functions and Parameters Used for the Clutter Recognition

Membership Function	Function Type	Parameter	Parameter	Parameter
Small	Bell-shaped	$a = 575$	$b = 3.12$	$c = 0$
Middle	Gaussian	$\sigma = 190$	$c = 1000$	
Large	Gaussian	$\sigma = 204$	$c = 1020$	

Table A5. "SNR Score" Output Membership Functions and Parameters Used for the SNR Score Recognition

Membership Function	Function Type	Parameter	Parameter
Min	Gaussian	$\sigma = 360$	$c = 0$
Max	Gaussian	$\sigma = 110$	$c = 1010$

Table A6. "Spectral Width" Membership Functions and Parameters Used for the Spectral Width Score Recognition

Membership Function	Function Type	Parameter	Parameter
Min	Z-shaped	$a = 53$	$b = 441.5$
Max	Z-shaped	$a = 989$	$b = 1004$

Table A7. "SNR" Membership Functions and Parameters Used for the Spectral Width Score Recognition

Membership Function	Function Type	Parameter	Parameter
Min	Gaussian	$\sigma = 354$	$c = 0.8$
Max	Gaussian	$\sigma = 100$	$c = 1010$

Table A8. "Spectral Width Score" Output Membership Functions and Parameters Used for the Spectral Width Score Recognition

Membership Function	Function Type	Parameter	Parameter
Small	Gaussian	$\sigma = 321$	$c = 0.5$
Middle	Gaussian	$\sigma = 415.3$	$c = 36$

Table A9. "Vertical Wind Speed" Membership Functions and Parameters Used for the Vertical Velocity Score Recognition

Membership Function	Function Type	Parameter	Parameter
Min	Gaussian	$\sigma = 40$	$c = 10$
Max	Gaussian	$\sigma = 200$	$c = 58$

Table A10. "Variance of Vertical Velocity" Membership Functions and Parameters Used for the Vertical Velocity Score Recognition

Membership Function	Function Type	Parameter	Parameter
Small	Gaussian	$\sigma = 10$	$c = 1$
Large	Gaussian	$\sigma = 20$	$c = 6$

Table A11. "Vertical Velocity Score" Output Membership Functions and Parameters Used for the Vertical Velocity Score Recognition

Membership Function	Function Type	Parameter	Parameter
Min	Gaussian	$\sigma = 36$	$c = 0$
Max	Gaussian	$\sigma = 50$	$c = 100$

2. Spectral width score recognition algorithm

In the spectral width score recognition algorithm, spectral width, RCSNR, and spectral width score output are computed using Z-shaped and Gaussian membership functions. For computing spectral width, Z-shaped membership functions, and RCSNR and spectral width score, Gaussian membership functions are used.

Spectral width score rules

1. If spectral width is maximum and SNR is maximum, then spectral width score is maximum.
2. If spectral width is minimum, then spectral width score is minimum.
3. If spectral width is maximum, then spectral width score is maximum.
4. If SNR is maximum, then spectral width score is maximum.
5. If SNR is minimum, then spectral width score is minimum.

3. Vertical velocity score recognition algorithm

In the vertical velocity score recognition algorithm, vertical wind speed and variance of vertical velocity are the inputs and vertical velocity score is the output, computed using Gaussian membership functions.

Vertical velocity score rules

1. If vertical wind speed is maximum, then vertical velocity score is maximum (optional: if early night hours present postsunset phenomenon).
2. If vertical wind speed is minimum, then vertical velocity score is minimum (optional: if early night hours present postsunset phenomenon).
3. If variance of vertical wind is large, then vertical velocity score is minimum.
4. If variance of vertical wind is small, then vertical velocity score is maximum.

Acknowledgments
The authors wish to thank M. Venkat Ratnam from the National Atmospheric Laboratory, Gadanki, India, for providing the GPS RS data. The authors thank M. Parandhamaiah from the Department of Physics, S.V. University, Tirupati, India, for his valuable suggestions and advice. This work was supported by the Korea Institute of Civil Engineering and Building Technology Strategic Research Project (Development of Driving Environment Observation, Prediction and Safety Technology Based on Automotive Sensors). We also thank three anonymous reviewers and the Editor for their insightful comments that improved the manuscript. The data used in this study are available and can be provided by registering/requesting at https://www.narl.gov.in/ or can be provided upon request to P. Yasodha (pyasoda@narl.gov.in—radar data) and M. Venkat Ratnam (vratnam@narl.gov.in—radiosonde data).

References

Allabakash, S., P. Yasodha, L. Bianco, S. Venkatramana Reddy, and P. Srinivasulu (2015a), Improved moments estimation for VHF active phased array radar using fuzzy logic method, *J. Atmos. Ocean. Technol.*, *32*, 1004–1014.

Allabakash, S., P. Yasodha, S. Venkatramana Reddy, and P. Srinivasulu (2015b), Wavelet transform based methods for removal of ground clutter and denoising the radar wind profiler data, *J. IET Signal Process.*, *9*, 440–448.

Anandan, V. K., P. Balamurlidhar, P. B. Rao, A. R. Jain, and C. J. Pan (2005), An adaptive moments estimation technique applied to MST radar echoes, *J. Atmos. Ocean. Technol.*, *22*, 396–408, doi:10.1175/JTECH1696.1.

Angevine, W. M., A. B. White, and S. K. Avery (1994), Boundary layer depth and entrainment zone characterization with a boundary-layer profiler, *Boundary Layer Meteorol.*, *68*, 375–385.

Basha, G., and M. Venkat Ratnam (2009), Identification of atmospheric boundary layer height over a tropical station using high-resolution radiosonde refractivity profiles: Comparison with GPS radio occultation measurements, *J. Geophys. Res.*, *114*, D16101, doi:10.1029/2008JD011692.

Barth, M. F., R. B. Chadwick, and D. W. van de Kamp (1994), Data processing algorithms used by NOAA's Wind Profiler Demonstration Network, *Ann. Geophys.*, *12*, 518–528, doi:10.1007/s00585-994-0518-1.

Bianco, L., and J. M. Wilczak (2002), Convective boundary layer depth: Improved measurement by Doppler radar wind profiler using fuzzy logic methods, *J. Atmos. Ocean. Technol.*, *19*, 1745–1758, doi:10.1175/1520-0426(2002)019,1745:CBLDIM.2.0.CO;2.

Bianco, L., I. V. Djalalova, C. W. King, and J. M. Wilczak (2011), Diurnal evolution and annual variability of boundary layer height and its correlation to other meteorological variables in California's central valley, *Boundary Layer Meteorol.*, *140*, 491–511, doi:10.1007/s10546-011-9622-4.

Bianco, L., J. M. Wilczak, and A. B. White (2008), Convective boundary layer depth estimation from wind profilers: Statistical comparison between an automated algorithm and expert estimations, *J. Atmos. Ocean. Technol.*, *25*, 1397–1413, doi:10.1175/2008JTECHA981.1.

Carter, D., K. S. Gage, W. L. Ecklund, W. M. Angevine, P. M. Johnston, A. C. Riddle, J. Wilson, and C. R. Williams (1995), Development in UHF lower tropospheric wind profiling at NOAA's Aeronomy Laboratory, *Radio Sci.*, *30*, 977–1001, doi:10.1029/95RS00649.

Contini, D., G. Mastrantonio, A. Viola, and S. Argentini (2004), Mean vertical motions in the PBL measured by Doppler Sodar: Accuracy, ambiguities, and possible improvements, *J. Atmos. Ocean. Technol.*, *21*, 1532–1544.

Cornman, L. B., R. K. Goodrich, C. S. Morse, and W. L. Ecklund (1998), A fuzzy logic method for improved moment estimation from Doppler spectra, *J. Atmos. Ocean. Technol.*, *15*, 1287–1305, doi:10.1175/1520-0426(1998)015,1287:AFLMFI.2.0.CO;2.

Coulter, R. L. (1979), A comparison of three methods for measuring mixing layer height, *J. Appl. Meteorol.*, *18*, 1495–1499.

Emeis, S., C. Münkel, S. Vogt, W. J. Müller, and K. Schäfer (2004), Atmospheric boundary-layer structure from simultaneous SODAR, RASS, and ceilometer measurements, *Atmos. Environ.*, *38*(2), 273–286.

Fairall, C. W. (1991), The humidity and temperature sensitivity of clear-air radars in the convective boundary layer, *J. Appl. Meteorol.*, *30*, 1064–1074.

Gamo, M., P. Goyal, M. Kumari, U. C. Mohanty, and M. P. Singh (1994), Mixed-layer characteristics as related to the monsoon climate of New Delhi, India, *Boundary Layer Meteorol.*, *67*, 213–227.

Garratt, J. R. (1992), *The Atmospheric Boundary Layer*, Cambridge Atmospheric and Space Science Series, vol. 416, p. 444, Cambridge Univ. Press, Cambridge.

Hildebrand, P. H., and R. S. Sekhon (1974), Objective determination of the noise level in Doppler spectra, *J. Appl. Meteorol.*, *13*, 808–811, doi:10.1175/1520-0450(1974)013,0808:ODOTNL.2.0.CO;2.

Indian meteorological Department monsoon report (2011). [Available at http://www.imd.gov.in/section/nhac/dynamic/monsoon_report_2011.pdf.]

Indian meteorological Department monsoon report (2013). [Available at http://www.imd.gov.in/section/nhac/dynamic/monsoon_report_2013.pdf.]

Jordan, J. R., R. J. Lataitis, and D. A. Carter (1997), Removing ground and intermittent clutter contamination from wind profiler signals using wavelet transforms, *J. Atmos. Ocean. Technol.*, *14*, 1280–1297, doi:10.1175/1520-0426(1997)014,1280:RGAICC.2.0.CO;2.

Kalapureddy, M. C. R., K. K. Kumar, V. Sivakumar, A. K. Ghosh, A. R. Jain, and K. K. Reddy (2007), Diurnal and seasonal variability of TKE dissipation rate in the ABL over a tropical station using UHF wind profiler, *J. Atmos. Sol. Terr. Phys.*, *69*, 419–430.

Klir, G. J., U. St Clair, and B. Yuan (1997), *Fuzzy Set Theory: Foundations and Applications*, Prentice-Hall, New Jersey.

Kohler, M., N. Kalthoff, and C. Kottmeier (2010), The impact of soil moisture modifications on CBL characteristics in West Africa: A case-study from the AMMA campaign, *Q. J. R. Meteorol. Soc.*, *136*, 442–455.

Krishnan, P., P. K. Kunhikrishnan, S. M. Nair, S. Ravindran, A. R. Jain, and T. Kozu (2003), Atmospheric boundary layer observations over Gadanki using lower atmospheric wind profiler: Preliminary results, *J. Curr. Sci.*, *85*(1), 75–79.

Krishnamurti, T. N., and Y. Ramanathan (1982), Sensitivity of the monsoon onset to differential heating, *J. Atmos. Sci.*, *39*, 1290–1306.

Kumar, K. K., and A. R. Jain (2006), L band wind profiler observations of convective boundary layer over Gadanki, India (13.5_N, 79.2_E), *Radio Sci.*, *41*, RS2004, doi:10.1029/2005RS003259.

Lehmann, V., and G. Teschke (2001), Wavelet based methods for improved wind profiler signal processing, *Ann. Geophys.*, *19*, 825–836, doi:10.5194/angeo-19-825-2001.

Lehtinen, R., and J. Jordan (2006), Improving wind profiler measurements exhibiting clutter contamination using wavelet transforms. Preprints, WMO Tech. Conf. on Meteorological and Environmental Instruments and Methods of Observation (TECO-2006), Geneva, Switzerland, WMO, P2.20. [Available at http://www.wmo.int/pages/prog/www/IMOP/publications/IOM-94-TECO2006/P2(20)_Lehtinen_USA.pdf.]

Levi, Y., E. Shilo, and I. Setter (2011), Climatology of a summer coastal boundary layer with 1290-MHz wind profiler radar and a WRF simulation, *J. Appl. Meteorol. Climatol.*, *50*, 1815–1826.

Manjula, G., M. Roja Raman, M. Venkat Ratnam, A. V. Chandrasekhar, and S. Vijaya Bhaskara Rao (2016), Diurnal variation of ducts observed over a tropical station, Gadanki using high-resolution GPS radiosonde observations, *Radio Sci.*, *51*, 247–258, doi:10.1002/2015RS005814.

Matlab fuzzy logic toolbox (2013), Users guide, R. [Available at www.mathworks.in/help/pdf_doc/fuzzy/fuzzy.pdf.]

McCaffrey, K., L. Bianco, and J. M. Wilczak (2016), Improved observations of turbulence dissipation rates from wind profiling radars, *Atmos. Meas. Tech. Discuss.*, doi:10.5194/amt-2016-322,2016.

Medeiros, B., A. Hall, and B. Stevens (2005), What controls the mean depth of the PBL?, *J. Clim.*, *18*(16), 3157–3172.

Merritt, D. A. (1995), A statistical averaging method for wind profiler Doppler spectra, *J. Atmos. Oceanic Technol.*, *12*(5), 985–995.

Morse, C. S., R. K. Goodrich, and L. B. Cornman (2002), The NIMA method for improved moment estimation from Doppler spectra, *J. Atmos. Ocean. Technol.*, *19*, 274–295, doi:10.1175/1520-0426-19.3.274.

Rao, T. N., D. N. Rao, K. Mohan, and S. Raghavan (2001), Classification of tropical precipitating systems and associated Z-R relationships, *J. Geophys. Res.*, *106*(D16), 17,699–17,711.

Reddy, K. K., et al. (2001), Lower atmospheric wind profiler at Gadanki, tropical India: Initial results, *Meteorol. Z.*, *10*, 457–468.

Reddy, K. K., et al. (2002), Planetary boundary layer and precipitation studies using lower atmospheric wind profiler over tropical India, *J. Radio Sci.*, *37*, 4, doi:10.1029/2000RS002538.

Reddy, K. K., T. Kozu, and D. N. Rao (2006), Wind profiler radar for understanding the tropical convective boundary layer during different seasons, *Indian J. Radio Space Phys.*, *35*, 105–115.

Reddy, K. K., M. Naja, N. Ojha, P. Mahesh, and S. Lal (2012), Influences of the boundary layer evolution on surface ozone variations at a tropical rural site in India, *J. Earth Syst. Sci.*, *121*(4), 911–922.

Reno, M. J., C. W. Hansen, and J. S. Stein (2012), *Global Horizontal Irradiance Clear Sky Models: Implementation and Analysis*, SAND2012-2389, Sandia National Laboratories, Albuquerque, N. M.

Riddle, A. C., and W. M. Angevine (1992), Ground clutter removal from profiler spectra, in *Proceedings of the Fifth Workshop on Technical and Scientific Aspects of MST Radar*, Aberystwyth, Wales, United Kingdom, URSI/SCOSTEP 418–420.

Sandeep, A., T. N. Rao, C. N. Ramkiran, and S. V. B. Rao (2014), Differences in atmospheric boundary-layer characteristics between wet and dry episodes of the Indian summer monsoon, *Boundary Layer Meteorol.*, *153*, 217–236.

Savitzky, A., and M. J. E. Golay (1964), Smoothing and differentiation of data by simplified least squares procedures, *Anal. Chem.*, *36*, 1627–1639.

Sivanandam, S. N., S. Sumathi, and S. N. Deepa (2007), *Introduction to Fuzzy Logic Using MATLAB*, Springer, Berlin.

Srinivasulu, P., P. Yasodha, P. Kamaraj, T. N. Rao, A. Jayaraman, S. N. Reddy, and S. Satyanarayana (2012), 1280-MHz active array radar wind profiler for lower atmosphere: System description and data validation, *J. Atmos. Ocean. Technol.*, *29*, 1455–1470, doi:10.1175/JTECH-D-12-00030.1.

Strauch, R. G., D. A. Merritt, K. P. Moron, K. B. Earnshaw, and D. W. van de Kamp (1984), The Colorado Wind-Profiling Network, *J. Atmos. Ocean. Technol.*, *1*, 37–49, doi:10.1175/1520-0426(1984)001,0037:TCWPN.2.0.CO;2.

Stull, R. B. (1988), *An Introduction to Boundary Layer Meteorology*, p. 666, Kluwer Acad., Norwell. Mass.

VanZandt, T. E., J. L. Green, K. S. Gage, and W. L. Clark (1978), Vertical profiles of reflectivity turbulence structure constant: Comparison of observations by the sunset radar with a new theoretical model, *Radio Sci.*, *13*, 819–829, doi:10.1029/RS013i005p00819.

White, A. B., C. W. Fairall, and D. W. Thompson (1991a), Radar observations of humidity variability in and above the marine atmospheric boundary layer, *J. Atmos. Ocean. Technol.*, *8*, 639–658.

White, A. B., C. W. Fairall, and D. W. Wolfe (1991b), Use of 915 MHz wind profiler data to describe the diurnal variability of the mixed layer, in *7th Joint Conference on Application of Air Pollution Meteorology with AWMA*, pp. 14–18, Am. Meteorol. Soc, New Orleans.

Woodman, R. F. (1985), Spectral moment estimation in MST radars, *Radio Sci.*, *20*, 1185–1195, doi:10.1029/RS020i006p01185.

Wyngaard, J. C., and M. A. LeMone (1980), Behavior of the refractive index structure parameter in the entraining convective boundary layer, *J. Atmos. Sci.*, *37*, 1573–1585.